Hindawi Publishing Corporation
Journal of Nanomaterials
Volume 2012, Article ID 252894, 11 pages
doi:10.1155/2012/252894

*Research Article*

# Impact of $Ge^{4+}$ Ion as Structural Dopant of $Ti^{4+}$ in Anatase: Crystallographic Translation, Photocatalytic Behavior, and Efficiency under UV and VIS Irradiation

**Václav Štengl,[1,2] Tomáš Matys Grygar,[1,2] Jana Velická,[1] Jiří Henych,[1,2] and Snejana Bakardjieva[1,2]**

[1] *Department of Solid State Chemistry, Institute of Inorganic Chemistry AS CR v.v.i., 250 68 Řež, Czech Republic*
[2] *Faculty of The Environment, University of Jan Evangelista Purkyně, Králova Výšina 7, 400 96 Ústí nad Labem, Czech Republic*

Correspondence should be addressed to Václav Štengl, stengl@iic.cas.cz

Received 24 March 2012; Revised 13 May 2012; Accepted 14 May 2012

Academic Editor: Jiaguo Yu



Nanometric particles of germanium-doped $TiO_2$ were prepared by homogeneous hydrolysis of $TiOSO_4$ and $GeCl_4$ in an aqueous solution using urea as the precipitation agent. Structural evolution during heating of these starting Ge-Ti oxide powders was studied by X-ray diffraction (XRD) and high-temperature X-ray powder diffraction (HTXRD). The morphology and microstructure changes were monitored by means of scanning electron microscopy (SEM), Raman and infrared spectroscopy (IR), specific surface area (BET), and porosity determination (BJH). The photocatalytic activity of all samples was determined by decomposition of Orange II dye under irradiation at 365 nm and 400 nm. Moderate doping with concentration upto value 2.05 wt.% positively influences azo dye degradation under UV and Vis light. Further improvement cannot be achieved by higher Ge doping. Effect of the annealing (200, 400, and 700°C) on photocatalysis and other properties has been assessed.

## 1. Introduction

$TiO_2$ photocatalyst is in the focus of numerous studies due to its attractive characteristics and application in the remediation of environmental contaminants, that is, water disinfection [1]. Despite its potential application, the fast recombination of photo-generated electron-hole pair on the surface or in the lattice of $TiO_2$ limits its practical use. Couple of strategies has been proposed to enhance the effectiveness of the photocatalysis. Recent techniques include, for instance, controlled structures with exposed active facets [2, 3]. However, doping of metal ions in $TiO_2$ is the widespread quite common technique to suppress the rate of that recombination. Doping of a metal ion in a semiconductor is known to affect both photophysical behavior and photochemical activity. Enhanced photocatalytic activity over binary metal oxides and transition metal, noble metal, or non-metal-doped $TiO_2$ has been widely reported [4–8]. Transition metal ion doping may improve the trapping of electrons and inhibit the electron-hole recombination [9]. The incorporation of germanium (Ge) into titania ($TiO_2$) creates an attractive semiconductor. $TiO_2$-Ge nanocomposite thin films were synthesized by RF magnetron sputtering from targets fabricated from a mixture of $TiO_2$ (P25 Degussa) and Ge powders [10]. Titania-germanium nanocomposite, which comprises Ge nanodots in the $TiO_2$ matrix, is an interesting thermoelectric [11], optoelectronic [12], and photovoltaic material [13, 14]. The preparation of titania ($TiO_2$), germania ($GeO_2$), and binary $TiO_2$-$GeO_2$ oxide gels with different Ti/Ge ratio gels based on sol-gel method with surfactant-assisted mechanism and their application for dye-sensitized solar cells were reported [15]. Adding a small amount of commercial $GeO_2$ into aqueous suspension significantly enhanced the photocatalytic activity of titania-based photocatalysts (P25) for the degradation of dyes [16].

In the present study a more cost-effective and environmentally friendly method is used for the photocatalyst preparation: homogenous precipitation of acid aqueous

solutions of $TiOSO_4$ with urea is applied to obtain Ge:$TiO_2$ nanocrystallites with the Ge content varying between 0 and 12 wt%. The set of eight samples with various amounts of Ge were prepared. Current attention has been focused on the influence of germanium incorporation into monodispersed spherical particles of anatase. The relationship between the photocatalytic activity of suspended nanocrystalline mixtures and their physical properties is discussed to understand a reasonable microstructure-activity relationship. The attention has been paid not only to crystal structures, but also to BET surface area, particle size, porosity, and the effect of the individual nanocrystallites on the photoactivity. The photocatalytic activity of the as-prepared doped titania was assessed by the photocatalytic decomposition of Orange II dye in an aqueous slurry under UV and Vis irradiation at wavelengths of 365 nm and 400 nm.

## 2. Experimental

*2.1. Preparation of Samples.* All chemical reagents used in the present experiments were obtained from commercial sources. $TiOSO_4$, $GeCl_4$, and urea were supplied by Sigma-Aldrich, Czech Republic.

Nanometric particles of doped titania were prepared by homogeneous hydrolysis of $TiOSO_4$ and $GeCl_4$ in aqueous solutions using urea as the precipitation agent. In a typical process, 100 g $TiOSO_4$ was dissolved in 100 mL hot distilled water acidified with 98% $H_2SO_4$. The pellucid liquid was diluted by 4 L distilled water and a defined amount of $GeCl_4$ was added using microsyringe (0 to 1 mL, Hamilton). The resulting solution was mixed with 300 g of urea (see Table 1) and heated at 100°C for 6 h under stirring until pH reached 7.2; at this pH gaseous ammonia is released from the mixture. The formed precipitates were decanted, filtered, and dried at 105°C. Eight new doped titania samples denoted as TiGeXX (where XX = 05, 07, 10, 15, 25, 30, 60, and 90 is the amount of $GeCl_4$ in mL) were prepared (see Table 1). In order to see how ion influences the structural alteration of anatase $TiO_2$ during heating, the whole set of samples was annealed at 200, 400, and 700°C in a muffle furnace with the temperature rate 10°C $min^{-1}$ during 2 hours.

*2.2. Characterization Methods.* Diffraction patterns were collected with diffractometer PANalytical X′Pert PRO equipped with conventional X-ray tube (Cu K$\alpha$ radiation, 40 kV, 30 mA) and a linear position sensitive detector PIXcel with an antiscatter shield. A programmable divergence slit set to a fixed value of 0.5 deg, soller slits of 0.02 rad, and mask of 15 mm were used in the primary beam. A programmable anti-scatter slit set to fixed value of 0.5 deg., Soller slit of 0.02 rad, and Ni beta-filter were used in the diffracted beam. Qualitative analysis was performed with the DiffracPlus Eva software package (Bruker AXS, Germany) using the JCPDS PDF-2 database [17]. For the quantitative analysis of XRD patterns we used Diffracplus Topas (Bruker AXS, Germany, version 4.1) with structural models based on ICSD database [18]. This program permits to estimate the weight fractions of crystalline phases and mean coherence length by means of Rietveld refinement procedure. The internal standard addition method with rutile (10 wt.%) was used for amorphous phase determination [19].

The sample TiGe09 was studied by *in situ* high temperature XRD in air with a PANalytical X'Pert PRO diffractometer using Co K radiation (40 kV, 30 mA) and a multichannel detector X'Celerator with an anti-scatter shield, equipped with a high temperature chamber (HTK 16, Anton Paar, Graz, Austria). The measurements started at room temperature and finished at 1200°C. The XRD measurements using rutile as an internal standard (10 wt.%) were performed to evaluate the content of amorphous phase in doped titania samples.

Scanning electron microscopy was performed with Quanta 200 FEG (high-resolution field emission gun SEM microscope, FEI Czech Republic) equipped with an energy dispersive X-ray spectrometer (EDS). Specimens for morphological investigations were prepared by droplet evaporation of samples dispersion on a carbon-supported SEM target. The specimens have been imaged in the low-vacuum mode using accelerating voltages of 30 kV.

The specific surface areas of samples were determined from nitrogen adsorption-desorption isotherms at liquid nitrogen temperature using a Coulter SA3100 instrument with outgas 15 min at 150°C. The Brunauer-Emmett-Teller (BET) method was used for surface area calculation [20]. The pore size distribution (pore diameter, pore volume, and micropore surface area of the samples) was determined by the Barrett-Joyner-Halenda (BJH) method [21].

Diffuse reflectance UV/VIS spectra for evaluation of photophysical properties were recorded in the diffuse reflectance mode ($R$) and transformed to absorption spectra using the Kubelka-Munk function [22]. A Perkin Elmer Lambda 35 spectrometer equipped with a Labsphere RSA-PE-20 integration sphere with $BaSO_4$ as a standard was used.

Raman spectra were obtained with DXR Raman microscope (Thermo Scientific, USA). 532 nm laser was used at a power set from 0.2 to 3 mW in aim to obtain optimal Raman signal. Powdered samples were scanned at 15-points mapping mode under 10x objective in an automated autofocus mode.

DTA-TG-MS measurements were carried out using a simultaneous Netzsch Instrument STA 409 coupled to quadrupole mass spectrometer Balzers QMS-420 under dynamic conditions in the air (flow rate 75 mL $min^{-1}$). The samples were heated at the rate of 3°C $min^{-1}$.

Photocatalytic activity of samples was assessed from the kinetics of the photocatalytic degradation of 0.02 M Orange II dye (sodium salt 4-[(2-hydroxy-1-naphtenyl)azo]-benzene-sulfonic acid) in aqueous slurries. The amount of the dye in the experiment by far exceeds the sorption capacity of the titania. For azo dye degradation, the complete mass balance in nitrogen indicated that the central –N=N– azo group was converted in gaseous dinitrogen, which is ideal for the elimination of nitrogen-containing pollutants, not only for environmental photocatalysis but also for any physicochemical method [23]. Direct photolysis employing artificial UV light or solar energy source cannot mineralize Orange II [24]. Kinetics of the photocatalytic degradation of

Table 1: The EDX analysis, surface area, porosity, crystallite size, anatase and amorphous phase contents, and cell parameters *a* and *c*.

| Sample | $GeCl^4$ [mL] | EDX Ge [wt.%] | Specific surface area [$m^2g^{-1}$] | Pore volume [$cm^3g^{-1}$] | Cryst. Size [nm] | Anatase [wt.%] | Amorph. phase [wt.%] | Cell param. *a* [Å] | Cell param. *c* [Å] |
|---|---|---|---|---|---|---|---|---|---|
| TiGe00 | 0.0 | 0.0 | 200.4 | 0.1905 | 13.4 | 83.8 | 16.2 | 3.7949 | 9.5065 |
| TiGe05 | 0.5 | 0.84 | 239.5 | 0.2616 | 14.7 | 77.1 | 22.9 | 3.7946 | 9.5013 |
| TiGe07 | 0.7 | 1.23 | 245.1 | 0.2640 | 14.9 | 76.6 | 23.4 | 3.7942 | 9.5003 |
| TiGe10 | 1.0 | 1.83 | 263.2 | 0.2239 | 11.3 | 78.2 | 21.8 | 3.7933 | 9.4996 |
| TiGe15 | 1.5 | 2.05 | 237.8 | 0.6039 | 14.8 | 74.1 | 25.9 | 3.7930 | 9.4981 |
| TiGe25 | 2.5 | 2.86 | 250.2 | 0.4065 | 13.1 | 77.1 | 22.9 | 3.7922 | 9.4950 |
| TiGe30 | 3.0 | 3.57 | 290.9 | 0.2255 | 9.8 | 78.2 | 21.8 | 3.7931 | 9.4920 |
| TiGe60 | 6.0 | 5.59 | 283.3 | 0.2404 | 10.5 | 81.3 | 18.7 | 3.7939 | 9.4988 |
| TiGe90 | 9.0 | 12.07 | 249.7 | 0.2232 | 11.5 | 65.3 | 34.7 | 3.7898 | 9.4768 |

aqueous Orange II dye solution was measured by using a self-constructed photoreactor [25]. The photoreactor consists of a stainless steel cover and quartz tube with fluorescent Narva lamp with power 13 W and light intensity ~3.5 $mWcm^{-2}$. Black light lamp (365 nm) for UV and warm white lamp (over 400 nm) for visible light irradiation were used. Orange II dye solution was circulated by means of membrane pump through a cell. The concentration of Orange II dye was determined by measuring absorbance at 480 nm with VIS spectrophotometer ColorQuest XE. The 0.5 g of titania sample was sonicated for 10 min with an ultrasonic bath (300 W, 35 kHz) before use. The pH of the resulting suspension was taken as the initial value for neutral conditions and under the experiment was kept at value 7.0.

## 3. Results and Discussions

*3.1. X-Ray Diffraction Analysis.* The XRD patterns of the doped titania samples are shown in Figure 1. Only the diffraction lines of anatase (ICDD PDF 21-1272) can be seen. The ionic radius 0.054 nm [26] is smaller than ionic radius of $Ti^{4+}$ (0.0605 nm) [27] and germanium can be easily substituted for $Ti^{4+}$ into $TiO_2$ lattice. The increasing germanium content leads to the tendency in prevalence of amorphous part phase. This phenomenon can influence the photocatalytic activity of as-prepared samples. The crystallite size, anatase and amorphous phase contents, and cell parameters *a* and *c* of anatase (calculated by Rietveld refinement) are presented in Table 1.

The high temperature XRD pattern of the sample TiGe90 (with the highest content of ion) is presented in Supplement Figure S1. of the Supplementary Material available online at doi:10.1155/2012/252894 The measurement started at room temperature and was completed at 1200°C with 50°C steps in temperature range 25–550°C and 25°C steps in the second temperature interval 550–1200°C. Diffraction lines of anatase (ICDD PDF 21-1272), rutile (ICDD PDF 21-1276), and GeO (ICDD PDF 30-0590) were observed during the heating. No diffraction lines of other phases were observed at temperatures up to 850°C (except for Pt sample holder diffraction lines), which means that is either noncrystalline (amorphous) or full incorporated into the anatase structure.

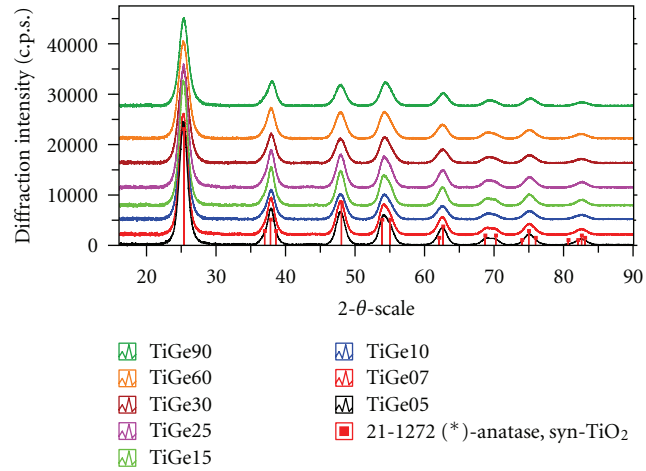


Figure 1: XRD patterns of prepared doped titania.

The temperatures above 850°C lead to the formation of crystalline GeO. The anatase-to-rutile transition begins at a higher temperature than in nondoped anatase; it starts at 900°C and continues up to 1000°C, which is by about 100°C higher than nondoped titania [28] and by about 500°C higher than Ru-doped titania [29].

As it was already mentioned, the thermodynamic stability of polymorphs depends on the crystallite size [30]. The temperature of the phase transition can be also understood as the temperature at which a critical crystallite size is achieved. The dependence of crystallite size on the temperature (see Supplement Figure S2a) shows that the phase transition of anatase begins when the crystallite size is ~68 nm. Compared with the results [28], the temperature shift by ~100°C for the anatase to rutile phase transition is associated with faster growth of the anatase crystallite size (see Supplement Figure S2b). The unit-cell parameters of the sample TiGe90 prepared by *in-situ* heating experiments increase almost linearly, which reflects the thermal expansion of the structures (see Supplement Figure S2c-d). An exception is the unit-cell parameter of anatase *a*, which decreases with increasing the temperature up to 600°C. This reduction is probably caused

by evolution of physically and chemically bounded water or other volatile structural impurity.

*3.2. Stoichiometry.* The doped titania samples were studied up to 800°C by simultaneous thermogravimetric and differential thermal analysis (TG/DTA). For results of the analysis of representative sample TiGe07 see Supplement Figure S5. Below 200°C, the weight loss is considered to be due to the escape of surface-bound water and/or carbon dioxide. The subsequent weight loss with the maximum rate at temperature 300°C is due to the escape of $CO_2$, which was possibly closed in the titania structure. Hydrolysis of urea leads to its degradation and *in situ* evolution of a large excess of $CO_2$ and $NH_3$. Ammonia reacts with water to form $NH_4OH$ and $CO_2$ effervesces from the reaction solution. The presence of ions leads to preferred sorption of $CO_2$ to titania surface, in contrast to $Ru^{3+}$ doping [31].

Because DTA-TG results indicated some thermal changes of the titania specimens, the prepared samples were heated at temperatures 200, 400, and 700°C to check a possible influence of the volatile admixtures on photocatalysis. The calcination was carried out in a laboratory muffle furnace with heating rate of 10°C $min^{-1}$; the desired temperature was kept for 2 hours. BET surface area and total pore volume of the calcines are listed in Supplement Table 2 and their photocatalytic activity in Table 1. At 200°C release of surface-bound water increases the specific surface area, but further annealing leads to its decrease as a consequence of growing particles size. In a dynamic experiment at the temperature around 300°C, $CO_2$ is released from the titania structure (see Supplement Figure S5) which is accompanied by modification of the mesoporous texture, pore size grows from 3 to ~5 nm (see Supplement Figure S6) for sample denoted TiGe07.

In order to see how incorporation influences the structural interchanges of anatase lattice and phase transition temperature of anatase to rutile modification all doped samples (where Ge content varying between 0.84–12 wt.%) have been heated at three different temperatures: 200, 400, and 700°C; three new sets of thermal treated samples were obtained (see Table 1). The calcination was carried out in a laboratory muffle furnace with rate of 10°C $min^{-1}$ and was kept 2 h at desired temperature.

*3.3. Surface Areas and Porosity.* The specific surface area of the as-prepared samples, calculated by the multipoint Brunauer-Emmett-Teller (BET) method, total pore volume, micropore surface area, and micropore volume are listed in Table 1. Barrett-Joyner-Halenda (BJH) pore-size distribution plot and nitrogen adsorption/desorption isotherms (inset) are shown in Figure 2 and are characteristic for all prepared samples. According to IUPAC notation [32], microporous materials have pore diameters < 2 nm and macroporous materials have pore diameters > 50 nm; the mesoporous category is in the middle. The mean pore size in the prepared photocatalysts is around ~3 nm and the pore size distribution is relatively narrow. All samples have a type IV isotherm, which is characteristic for mesoporous material with hysteresis, typical for large-pore mesoporous materials, and can be ascribed to capillary condensation in mesopores. The high steepness of the hysteresis indicates the high order of mesoporosity. All samples have type A hysteresis loop according de Boer's characterization [33]. This hysteresis type is connected with pores in the form of capillary tubes open at both ends, wide ink-bottle pores, and wedge-shaped capillaries.

The thermal treatment of the samples leads to changes of BET surface area, pore volume, and pore-size distribution. Although the samples calcined at various temperatures showed the same type of isotherm, the quantity of adsorbed nitrogen was found to be different for different temperatures. The nitrogen adsorption ability of the samples heated to 200°C showed an increasing trend in comparison with nonthermal-treated samples (see Supplement Table 2). In addition, the adsorption and desorption were found to cause a growth of large-pore volume at 200°C (except for the sample TiGe15) in relation with noncalcined series (see Table 1). The best microstructural properties at 200°C were achieved with the sample TiGe25 (2.86 wt.% ): this is attributed to the extremely high surface area (387.3 $m^2/g^{-1}$) and pore volume (0.4298 $cm^3/g^{-1}$) of that specimen. Further heat treatment (400°C) caused moderate reduction of both surface area and pore volume. Calcination performed at 700°C for 2 hours leads to inevitable decrease of surface area and pore volume: for instance the BET of TiGe05 sample (0.84% ) heated at that temperature is only 13.2 $m^2/g^{-1}$ and BJH is 0.0677 $cm^3/g^{-1}$. The surface area and pore volume data obtained for the samples calcined at various temperatures reveal that all samples can be used for photocatalysis except for the highest tested temperature (700°C). It is worth to mention that pore size showed an increasing trend with rise of the calcination temperature. The TiGe05 and TiGe07 samples heated at 200, 400, and 700°C showed a mesopore range of 5 nm and match well the characteristic of meso-structured materials. The mesoporous character of heated TiGe05-90 samples can be assigned to the synthetic parameters such as precipitation time, pH, temperature, and the annealing temperature. During the thermal treatment chemically and physically bound water and $CO_2$ are released and pores of larger radii are formed.

The SEM images of germanium-doped titania samples are presented in Figure 3. The titania powder consists of 2-3 $\mu$m spherical particles with a narrow particle size distribution. With increasing content, the size and shape of these spherical clusters remain unchanged and confirmed that structural alteration take place inside the spheres (see Table 1).

*3.4. Raman and IR Spectroscopy.* The Raman spectra of the samples are presented in Figure 4. The specific vibration modes are located around 151 $cm^{-1}$ (Eg), 399 $cm^{-1}$ (B1g), 515 $cm^{-1}$ (B1g + A1g), and 638 $cm^{-1}$ (Eg) indicating the presence of the anatase phase in all of these samples. The measured frequencies of peak positions vary between the samples, with increasing content of Ge at low frequency

Table 2: Photocatalytic activity of prepared doped titania samples.

| Sample | $k$ OII 365 nm [min$^{-1}$] | $k$ OII 400 nm [min$^{-1}$] | $k$ OII 365 nm at 200°C [min$^{-1}$] | $k$ OII 400 nm at 200°C [min$^{-1}$] | $k$ OII 365 nm at 400°C [min$^{-1}$] | $k$ OII 400 nm at 400°C [min$^{-1}$] | $k$ OII 365 nm at 700°C [min$^{-1}$] | $k$ OII 400 nm at 700°C [min$^{-1}$] |
|---|---|---|---|---|---|---|---|---|
| TiGe05 | 0.05783 | 0.00508 | 0.04258 | 0.00531 | 0.1204 | 0.00362 | 0.08167 | 0.00210 |
| TiGe07 | 0.07849 | 0.01456 | 0.07441 | 0.00793 | 0.07171 | 0.00473 | 0.09598 | 0.04299 |
| TiGe10 | 0.08118 | 0.00797 | 0.01868 | 0.00215 | 0.02592 | 0.00179 | 0.02283 | 0.00288 |
| TiGe15 | 0.08858 | 0.01530 | 0.07124 | 0.00543 | 0.07048 | 0.00382 | 0.01373 | 0.02349 |
| TiGe25 | 0.07989 | 0.01125 | 0.06095 | 0.00523 | 0.06525 | 0.00371 | 0.07858 | 0.02065 |
| TiGe30 | 0.01767 | 0.00160 | 0.01947 | 0.00233 | 0.01576 | 0.00270 | 0.02693 | 0.00439 |
| TiGe60 | 0.02177 | 0.00182 | 0.02883 | 0.00239 | 0.02698 | 0.00237 | 0.02773 | 0.00425 |
| TiGe90 | 0.01540 | 0.00205 | 0.01545 | 0.00249 | 0.01501 | 0.00224 | 0.01686 | 0.00310 |

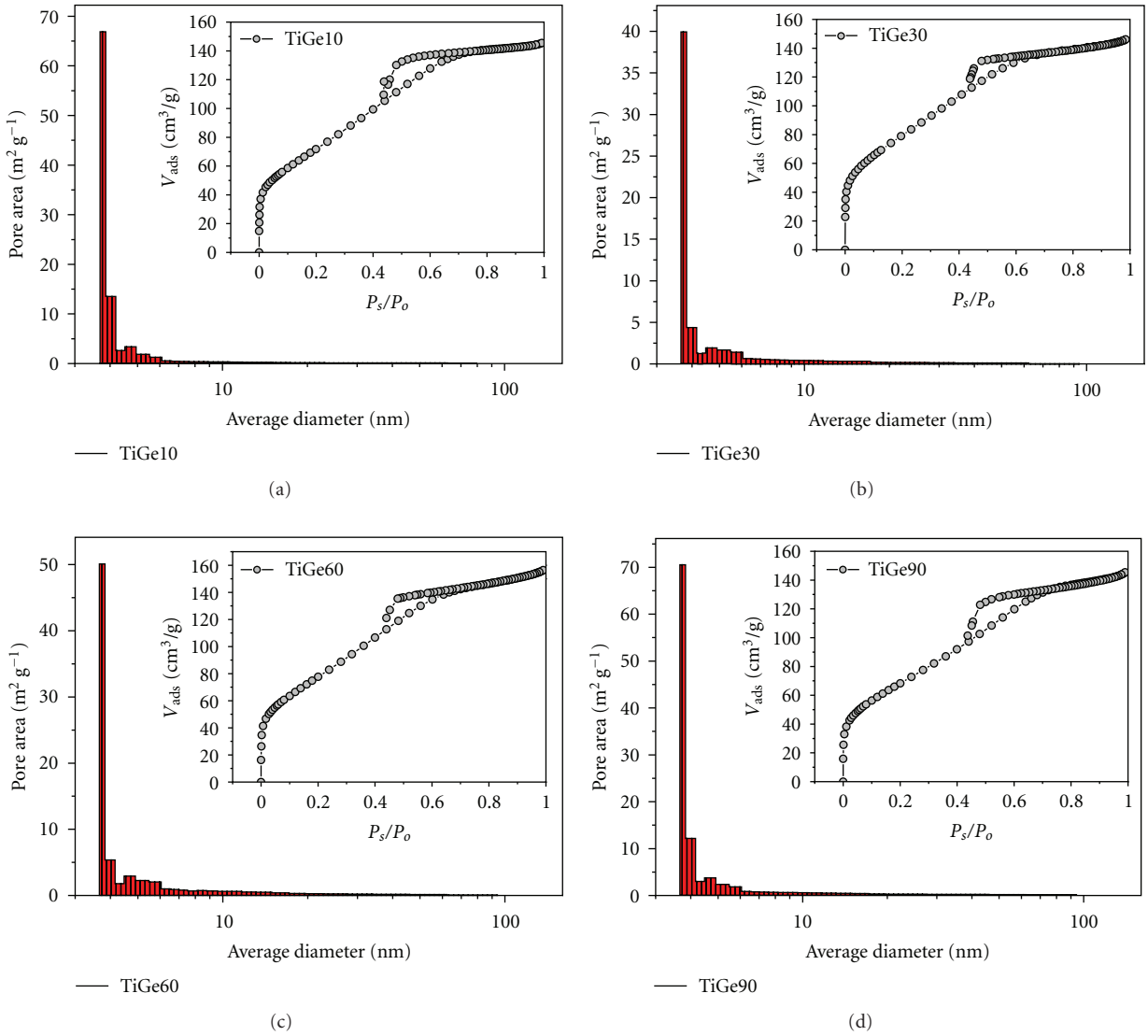


Figure 2: Pore area distribution of samples denoted as (a) TiGe10, (b) TiGe30, (c) TiGe60, and (d) TiGe90. Inset are hysteresis loops.

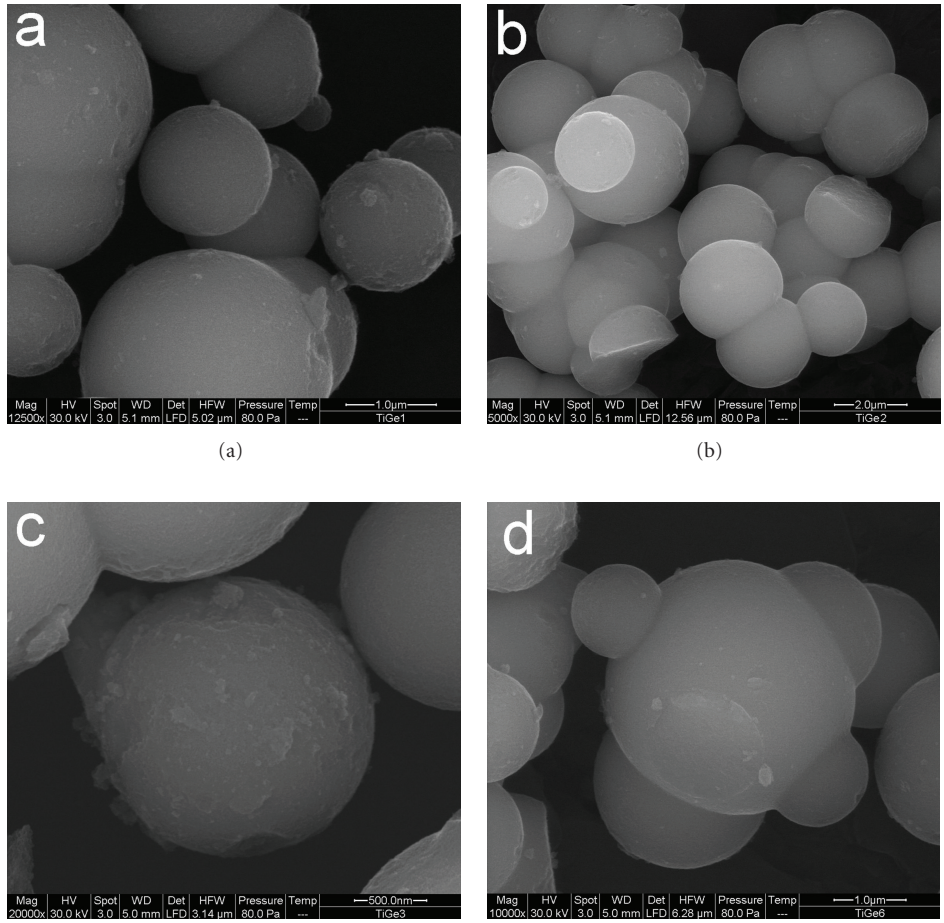


(a) (b)

(c) (d)

Figure 3: SEM images of prepared doped titania (a) TiGe10, (b) TiGe30 (c) TiGe60, and (d) TiGe90.

Eg mode shifts from 150.1 to 151.1 $cm^{-1}$ (see Supplement Table S1). Although this could be theoretically attributed to a change in the particle size, the shift of the position band of the Eg signal of the anatase signal should rather to some specific effect of the insertion into the $TiO_2$ framework or nonstoichiometry of titania be formed by the soft synthesis route.

Maximum of the Eg Raman band of annealed doped anatase specimen prepared by urea route is shifted by more than 6 $cm^{-1}$ with respect to pure anatase 144 $cm^{-1}$ [34, 35]. This shift is further continuously increasing by about 2 $cm^{-1}$ with growing Ge content up to the specimen 6 mL. The FWHM (the full width in the half maximum) of pure and Ge-doped anatase is as large as 23–28 $cm^{-1}$ with no obvious Ge concentration trend up to 6 mL $GeCl_4$ addition. Because XRD-estimated mean coherence length of the anatase is >10 nm, the shift of nondoped $TiO_2$ and large FWHM cannot be explained by phonon confinement due to limited particle size, for which particle size must have been <6 nm [34, 36]. The departure of the Raman band characteristics with respect to pure anatase must hence be attributed to nonstoichiometry, analogously as it was reported in the case of $CeO_2$ [37], and anatase [35] or other phenomena related to nonideal crystal lattice of anatase [38]. All prepared specimens can hence be considered as defective anatase, with minor but clear influence of Ge doping on the Eg band maximum.

Figure 5 shows the IR spectrum of the doped titania prepared by homogeneous hydrolysis with urea. The broad absorption peaks about 3400 $cm^{-1}$ and the band at 1623 $cm^{-1}$ correspond to the surface water and the hydroxyl groups [39]. The small band at ~1395 $cm^{-1}$ can be assigned to adsorbed carbonates on surfaces of $TiO_2$; $CO_2$ could have been originated from the urea decomposition [40]. Low frequency bands in the range <500 $cm^{-1}$ correspond to the Ti–O–Ti vibration of the network [41]. No other absorption bands were identified; therefore, the Ge atoms substitute Ti atoms in the all samples series TiGe.

*3.5. Diffuse Reflectance UV/Vis Spectroscopy.* Supplement Figure S3 presents UV/Vis absorption spectra of the doped $TiO_2$, nondoped $TiO_2$, and $GeO_2$. The anatase has a wide absorption band in the range from 200 to 385 nm and

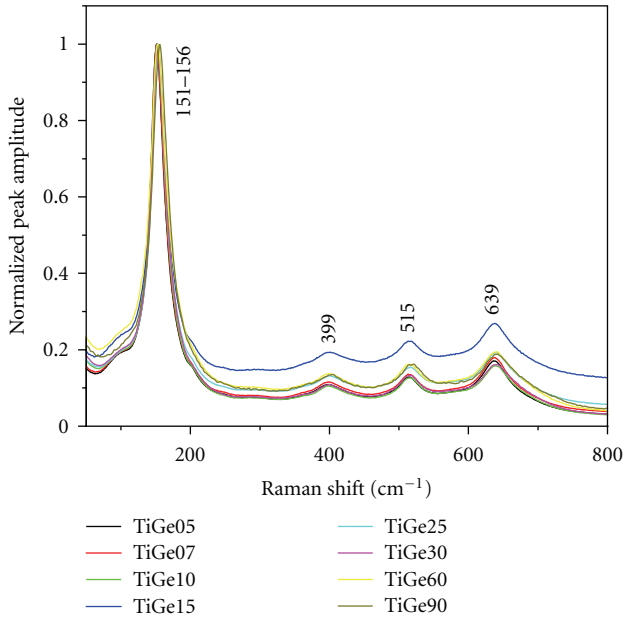


Figure 4: Raman spectra of prepared doped titania.

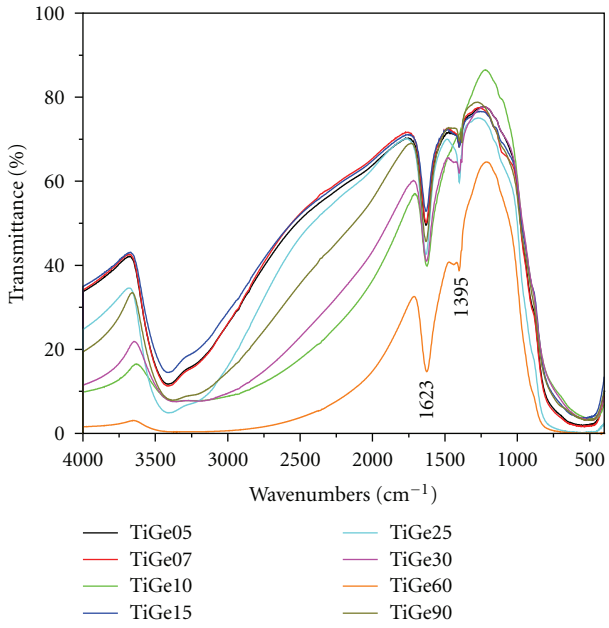


Figure 5: Infrared spectra of prepared doped titania.

the $GeO_2$ has a UV absorption band close to 325 nm. The diffuse reflectance spectra were transformed by performing the Kubelka-Munk transformation of the measured reflectance according to the following equation:

$$A(R) = \frac{(1-R)^2}{2R}, \tag{1}$$

where $R$ is the reflectance of an "infinitely thick" layer of the solid [42].

In comparison with the pure titania slight red shift of the absorption edge of doped samples is observed up to ~ 2,6 wt.% of. Conversely, with a further increase of Ge content the absorption edges are blue shifted. This could be caused perhaps by a presence of amorphous $GeO_2$ (see below).

The method of UV/Vis diffuse reflectance spectroscopy was employed to estimate the band-gap energies of the prepared germanium-doped $TiO_2$ samples. Firstly, to establish the type of band-to-band transition in these synthesized particles, the absorption data were fitted to equations for direct band-gap transitions. The minimum wavelength required to promote an electron depends upon the band-gap energy $E_{bg}$ which is commonly estimated from UV/Vis absorption spectra by the linear extrapolation of the absorption coefficient to zero using the following equation:

$$\alpha(h\nu) = A\left(h\nu - E_{bg}\right)^n, \tag{2}$$

where $A$ is the absorption according to (1), $B$ is absorption coefficient, and $h\nu$ is the photon energy in eV calculated from the wavelength $\lambda$ in nm [43, 44]:

$$h\nu = \frac{1239}{\lambda}. \tag{3}$$

In case that the fundamental absorption of the titania crystal possesses an indirect transitions between bands, then $n = 2$, for direct transition between bands $n = 1/2$ [45, 46]. The energy of the band gap is calculated by extrapolating a straight line to the abscissa axis, when $\alpha$ is zero, then $E_{bg} = h\nu$ [47]. Supplement Figure S4 shows the $(Ah\nu)^2$ versus photon energy for a direct band-gap transition. The value of 3.20 eV for sample denoted as TiGe0 is reported in the literature for pure anatase nanoparticles [46, 48]. The value of band-gap energy decreases only for sample denoted TiGe10 and TiGe15 (3.05 eV), in other samples is $E_{bg}$ in the range 3.1–3.2 eV. The band gap of bulk $GeO_2$ is 3.7 eV, which corresponds to absorption above approximately 350 nm. The decrease in band-gap of TiGe25, TiGe30, TiGe60, and TiGe90 is probably due to increased amount of amorphous phase $GeO_2$.

*3.6. Photocatalytic Tests.* According to the degradation pathway proposed in [49], the main byproducts formed by the ozonation of azo dye are organic acids, aldehydes, ketones, and carbon dioxide. Demirev and Nenov [50] suggested that the eventual degradation products of azo dye in the ozonation system would be acetic, formic, and oxalic acids. The reaction pathway for the visible light-driven photocatalytic degradation of Orange II dye in aqueous $TiO_2$ suspensions is schematically shown in [51].

On kinetics of heterogeneous photocatalysis for decomposition of model compounds such as dyes Orange II can be used Langmuir-Hinshelwood equation [52, 53]:

$$r = -\frac{d[\mathrm{OII}]}{dt} = -k \cdot K \cdot \frac{[\mathrm{OII}]}{1} + K \cdot [\mathrm{OII}], \tag{4}$$

where $r$ is the degree of dye mineralization, $k$ is the rate constant, $t$ is the illumination time, $K$ is the adsorption

coefficient of the dye, and [OII] is the dye concentration. At very low concentration of the dye, in the validity of Lambert-Beer Law [54]:

$$A = \varepsilon \cdot c \cdot l, \tag{5}$$

where $A$ is the absorbance, $c$, the dye concentration, $l$ the length of absorbent layer, and $\varepsilon$ is the molar absorption coefficient, it is possible to simplify (4) to the first order kinetic equation:

$$\ln\left(\frac{[\mathrm{OII}]}{[\mathrm{OII}]_0}\right) + K([\mathrm{OII}] - [\mathrm{OII}]_0) = -k \cdot K \cdot t \tag{6}$$

and after integration:

$$[\mathrm{OII}] = [\mathrm{OII}]_0 \cdot \mathrm{EXP}(-k_1 \cdot t); \quad (k_1 = k \cdot K). \tag{7}$$

The calculated degradation rate constants $k$ ($\mathrm{min}^{-1}$) for a reaction following the first order model kinetics of Orange II dye degradation at 365 nm (black light) and 400 nm (warm white light) are shown in Table 2 and the course of degradation is shown in Figure 6.

Moderate Ge doping up to the concentration 2.05 wt.% positively influences the azo dye degradation, but higher doping is not beneficial. The most active sample TiGe15 (containing 2.05 wt.%) is nonthermally treated and it has high contribution (74.1%) of very well-crystallized anatase nanocrystals with mean coherence length of 14-15 nm in a mixture with an amorphous phase (25.9%). The content has a positive effect on the porosity of titania. Higher level doping of reduces photocatalytic activity, probably due to decreasing particle size and total pore volume. A lower photocatalytic activity of TiGe30, TiGe60, and TiGe90 can be attributed to the content of amorphous phase of the germanium oxide and/or with a blue shift of the UV/VIS absorption edge (increase of $E_{bg}$). The contribution of Ge-amorphous phase can be expected to have significant influence, because the photocatalytic activity is lower compared to nondoped $TiO_2$ [55]. For the comparison of Ge-doped titania with other materials see Supplement Table S3.

All samples as received by wet synthesis as well as those annealed at the three calcination temperatures were subjected to the photocatalytic activity assessment. Thermal treatment affects surface area, pore size distribution, and porosity of the samples as mentioned above. Calcination at 200 and 400°C does not significantly affect the photocatalytic activity under 365 nm irradiation, while the activity under >400 nm irradiation decreased in most cases. Interestingly, the specific surface area and porosity of the catalysts increased after 200 and 400°C calcination. Obviously (and somehow surprisingly) these parameters are not the factors improving the titania photoactivity. Obviously the quality of the catalysts surface is deteriorated for the photodegradation under >400 nm irradiation. Calcination at so low temperatures cannot cause recrystallization or particle growth, and so we assume that dehydration/dehydroxylation of the titania surface could be responsible for that surface quality worsening. Indeed, TG/EGA analysis confirmed a loss of $H_2O$ < 150°C from the catalysts. This explanation is in agreement with the finding that photoactivity of titania obtained by a sol-gel route can be enhanced by the increase of the concentration of the surface hydroxyls [56]. Indeed, an oxygen overstoichiometry of titania specimens obtained by crystallization from aqueous solutions, which can only be rationalized by the presence of a pair $OH^-$ groups instead of one $O^{2-}$, has recently been confirmed by XPS analysis [57, 58].

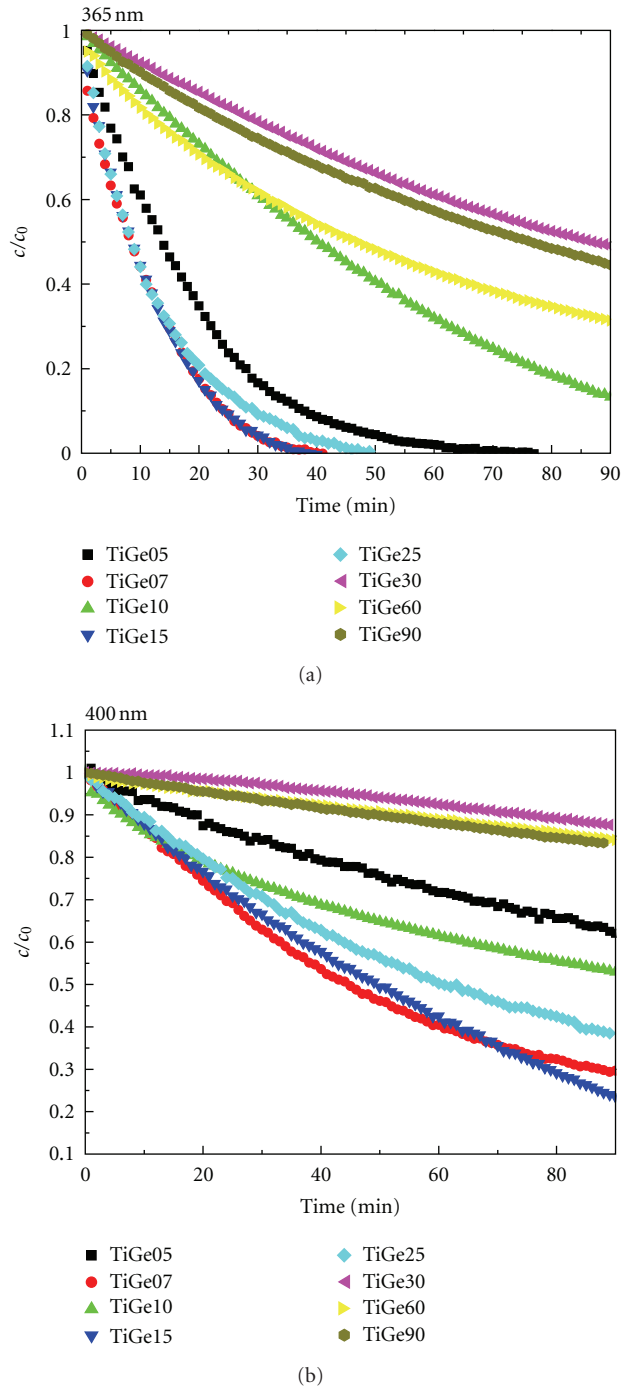


Figure 6: Photocatalytic activity of doped titania: (a) under $\lambda$ = 365 nm and (b) under $\lambda$ > 400 nm.

## 4. Conclusion

Small and moderate doping (0.84–2.65 wt.%) of titania has positively affected photocatalytic degradation of Orange II at both UV and Vis irradiations. The highest photocatalytic with TiGe15 sample (2.05 wt.%) with high contribution (74.1%) of very well-crystallized anatase nanocrystals and the BET surface area of 237.8 $m^2g^{-1}$. The pore size distribution measurement showed that this total surface area can be attributed mainly to mesopores with mean pore radius 5 nm.

The effect of the sample annealing at 200, 400, and 700°C was evaluated. 200°C annealing caused removal of surface-bound water and carbon dioxide, which resulted in a moderate increase of the surface area and the pore volume. However the photoactivity of the samples slightly decreased, probably as a consequence of the surface dehydroxylation of titania. Thermal treatment at higher temperatures (400 and 700°C) leads to a linear decrease of the surface area and the pore volume and resulted in lowering the photoactivity. The best photocatalytic activity in the entire set of thermally treated series was achieved with samples TiGe07/200, TiGe07/400, and TiGe07/700 (1.23 wt.%).

## Acknowledgments

This work was supported by the RVO 61388980 and the research work of J. Henych was financially supported by ENVIMOD Project (CZ.1.07/2.2.00/28.0205) by Ministry of Education, Youth and Sports of the Czech Republic. Petr Bezdička, Monika Maříková, and Eva Večerníková (all from Institute of Inorganic Chemistry AS CR) kindly performed a part of XRD measurements, IR, and thermal analyses, respectively.

## References

[1] J. A. Byrne, P. A. Fernandez-Ibañez, P. S. M. Dunlop, D. M. A. Alrousan, and J. W. J. Hamilton, "Photocatalytic enhancement for solar disinfection of water: a review," *International Journal of Photoenergy*, vol. 2011, Article ID 798051, 12 pages, 2011.

[2] S. W. Liu, J. G. Yu, and M. Jaroniec, "Anatase $TiO_2$ with dominant high-energy 001 facets: synthesis, properties, and applications," *Chemistry of Materials*, vol. 23, no. 18, pp. 4085–4093, 2011.

[3] S. W. Liu, J. G. Yu, and M. Jaroniec, "Tunable photocatalytic selectivity of hollow $TiO_2$ microspheres composed of anatase polyhedra with exposed 001 facets," *Journal of the American Chemical Society*, vol. 132, no. 34, pp. 11914–11916, 2010.

[4] W. Y. Choi, A. Termin, and M. R. Hoffmann, "The role of metal ion dopants in quantum-sized $TiO_2$: correlation between photoreactivity and charge carrier recombination dynamics," *Journal of Physical Chemistry*, vol. 98, no. 51, pp. 13669–13679, 1994.

[5] C. Anderson and A. J. Bard, "Improved photocatalytic activity and characterization of mixed $TiO_2/SiO_2$ and $TiO_2/Al_2O_3$ materials," *Journal of Physical Chemistry B*, vol. 101, no. 14, pp. 2611–2616, 1997.

[6] H. Znad, M. H. Ang, and M. O. Tade, "Ta/$TiO_2$-and Nb/$TiO_2$-mixed oxides as efficient solar photocatalysts: preparation, characterization, and photocatalytic activity," *International Journal of Photoenergy*, vol. 2012, Article ID 548158, 9 pages, 2012.

[7] X. F. Zhou, J. Lu, L. H. Li, and Z. S. Wang, "Preparation of crystalline sn-doped $TiO_2$ and its application in visible-light photocatalysis," *Journal of Nanomaterials*, vol. 2011, Article ID 432947, 5 pages, 2011.

[8] Q. J. Xiang, J. G. Yu, W. G. Wang, and M. Jaroniec, "Nitrogen self-doped nanosized $TiO_2$ sheets with exposed 001 facets for enhanced visible-light photocatalytic activity," *Chemical Communications*, vol. 47, no. 24, pp. 6906–6908, 2011.

[9] A. Di Paola, E. García-López, S. Ikeda, G. Marci, B. Ohtani, and L. Palmisano, "Photocatalytic degradation of organic compounds in aqueous systems by transition metal doped polycrystalline $TiO_2$," *Catalysis Today*, vol. 75, no. 1, pp. 87–93, 2002.

[10] S. Chatterjee, "Titania-germanium nanocomposite for photo-thermo-electric application," *Nanotechnology*, vol. 19, no. 26, Article ID 265701, 2008.

[11] S. Chatterjee, "Titania-germanium nanocomposite as a thermoelectric material," *Materials Letters*, vol. 62, no. 4-5, pp. 707–710, 2008.

[12] S. Chatterjee, "The optoelectronic properties of titania-germanium nanocomposites," *Journal of Physics D*, vol. 41, no. 5, Article ID 055301, 2008.

[13] S. Chatterjee, A. Goyal, and S. I. Shah, "Inorganic nanocomposites for the next generation photovoltaics," *Materials Letters*, vol. 60, no. 29-30, pp. 3541–3543, 2006.

[14] S. Chatterjee, "Titania-germanium nanocomposite as a photovoltaic material," *Solar Energy*, vol. 82, no. 2, pp. 95–99, 2008.

[15] A. Kitiyanan, T. Kato, Y. Suzuki, and S. Yoshikawa, "The use of binary $TiO_2$-$GeO_2$ oxide electrodes to enhanced efficiency of dye-sensitized solar cells," *Journal of Photochemistry and Photobiology A*, vol. 179, no. 1-2, pp. 130–134, 2006.

[16] J. Wang, Y. He, J. Tao et al., "Enhanced photodegradation of dyes on titania-based photocatalysts by adding commercial $GeO_2$ in aqueous suspension," *Chemical Communications*, vol. 46, no. 29, pp. 5250–5252, 2010.

[17] JCPDS, PDF 2 database, Release 50, International Centre for Diffraction Data, Newtown Square, volume 2000.

[18] ICSD, ICSD Database FIZ Karlsruhe, Germany, volume 2008.

[19] J. Środoń, V. A. Drits, D. K. McCarty, J. C. C. Hsieh, and D. D. Eberl, "Quantitative X-ray diffraction analysis of clay-bearing rocks from random preparations," *Clays and Clay Minerals*, vol. 49, no. 6, pp. 514–528, 2001.

[20] S. Brunauer, P. H. Emmett, and E. Teller, "Adsorption of gases in multimolecular layers," *Journal of the American Chemical Society*, vol. 60, no. 2, pp. 309–319, 1938.

[21] E. P. Barrett, L. G. Joyner, and P. P. Halenda, "The determination of pore volume and area distributions in porous substances. I. Computations from nitrogen isotherms," *Journal of the American Chemical Society*, vol. 73, no. 1, pp. 373–380, 1951.

[22] Z. C. Orel, M. K. Gunde, and B. Orel, "Application of the Kubelka-Munk theory for the determination of the optical properties of solar absorbing paints," *Progress in Organic Coatings*, vol. 30, no. 1-2, pp. 59–66, 1997.

[23] H. Lachheb, E. Puzenat, A. Houas et al., "Photocatalytic degradation of various types of dyes (Alizarin S, Crocein Orange G, Methyl Red, Congo Red, Methylene Blue) in water by UV-irradiated titania," *Applied Catalysis B*, vol. 39, no. 1, pp. 75–90, 2002.

[24] J. M. Monteagudo and A. Durán, "Fresnel lens to concentrate solar energy for the photocatalytic decoloration and mineralization of orange II in aqueous solution," *Chemosphere*, vol. 65, no. 7, pp. 1242–1248, 2006.

[25] V. Štengl, V. Houšková, S. Bakardjieva, N. Murafa, and V. Havlín, "Optically transparent titanium dioxide particles incorporated in poly(hydroxyethyl methacrylate) thin layers," *Journal of Physical Chemistry C*, vol. 112, no. 50, pp. 19979–19985, 2008.

[26] Y. Song, B. H. Bac, Y. B. Lee et al., "Ge-incorporation into 6-line ferrihydrite nanocrystals," *CrystEngComm*, vol. 12, no. 7, pp. 1997–2000, 2010.

[27] R. C. Pullar, S. J. Penn, X. Wang, I. M. Reaney, and N. M. Alford, "Dielectric loss caused by oxygen vacancies in titania ceramics," *Journal of the European Ceramic Society*, vol. 29, no. 3, pp. 419–424, 2009.

[28] S. Bakardjieva, J. Šubrt, V. Štengl, M. J. Dianez, and M. J. Sayagues, "Photoactivity of anatase-rutile $TiO_2$ nanocrystalline mixtures obtained by heat treatment of homogeneously precipitated anatase," *Applied Catalysis B*, vol. 58, no. 3-4, pp. 193–202, 2005.

[29] V. Houšková, V. Štengl, S. Bakardjieva, N. Murafa, and V. Tyrpekl, "Efficient gas phase photodecomposition of acetone by Ru-doped Titania," *Applied Catalysis B*, vol. 89, no. 3-4, pp. 613–619, 2009.

[30] H. Z. Zhang and J. F. Banfield, "Understanding polymorphic phase transformation behavior during growth of nanocrystalline aggregates: insights from $TiO_2$," *Journal of Physical Chemistry B*, vol. 104, no. 15, pp. 3481–3487, 2000.

[31] V. Houšková, V. Štengl, S. Bakardjieva, N. Murafa, and V. Tyrpekl, "Efficient gas phase photodecomposition of acetone by Ru-doped Titania," *Applied Catalysis B*, vol. 89, no. 3-4, pp. 613–619, 2009.

[32] S. Lowell and J. E. Shields, *Powder Surface Area and Porosity*, London, UK, 1998.

[33] J. A. de Boer, *Structure & Properties of Porous Materials*, Butterworths, London, UK, 1958.

[34] A. K. Arora, M. Rajalakshmi, T. R. Ravindran, and V. Sivasubramanian, "Raman spectroscopy of optical phonon confinement in nanostructured materials," *Journal of Raman Spectroscopy*, vol. 38, no. 6, pp. 604–617, 2007.

[35] S. Sahoo, A. K. Arora, and V. Sridharan, "Raman line shapes of optical phonons of different symmetries in anatase $TiO_2$ nanocrystals," *The Journal of Physical Chemistry C*, vol. 113, no. 39, pp. 16927–16933, 2009.

[36] S. Balaji, Y. Djaoued, and J. Robichaud, "Phonon confinement studies in nanocrystalline anatase-$TiO_2$ thin films by micro Raman spectroscopy," *Journal of Raman Spectroscopy*, vol. 37, no. 12, pp. 1416–1422, 2006.

[37] I. Kosacki, T. Suzuki, H. U. Anderson, and P. Colomban, "Raman scattering and lattice defects in nanocrystalline $CeO_2$ thin films," *Solid State Ionics*, vol. 149, no. 1-2, pp. 99–105, 2002.

[38] C. Lejon and L. Österlund, "Influence of phonon confinement, surface stress, and zirconium doping on the Raman vibrational properties of anatase $TiO_2$ nanoparticles," *Journal of Raman Spectroscopy*, vol. 42, no. 11, pp. 2026–2035, 2011.

[39] G. S. Shao, X. J. Zhang, and Z. Y. Yuan, "Preparation and photocatalytic activity of hierarchically mesoporous-macroporous $TiO_2$-xNx," *Applied Catalysis B*, vol. 82, no. 3-4, pp. 208–218, 2008.

[40] P. A. Connor, K. D. Dobson, and A. J. McQuillan, "Infrared spectroscopy of the $TiO_2$/aqueous solution interface," *Langmuir*, vol. 15, no. 7, pp. 2402–2408, 1999.

[41] G. Soler-Illia, A. Louis, and C. Sanchez, "Synthesis and characterization of mesostructured titania-based materials through evaporation-induced self-assembly," *Chemistry of Materials*, vol. 14, no. 2, pp. 750–759, 2002.

[42] A. A. Christy, O. M. Kvalheim, and R. A. Velapoldi, "Quantitative analysis in diffuse reflectance spectrometry: a modified Kubelka-Munk equation," *Vibrational Spectroscopy*, vol. 9, no. 1, pp. 19–27, 1995.

[43] K. M. Reddy, S. V. Manorama, and A. R. Reddy, "Bandgap studies on anatase titanium dioxide nanoparticles," *Materials Chemistry and Physics*, vol. 78, no. 1, pp. 239–245, 2003.

[44] J. Tauc, R. Grigorov, and A. Vancu, "Optical properties and electronic structure of amorphous germanium," *Physica Status Solidi*, vol. 15, no. 2, pp. 627–637, 1966.

[45] D. Reyes-Coronado, G. Rodríguez-Gattorno, M. E. Espinosa-Pesqueira, C. Cab, R. de Coss, and G. Oskam, "Phase-pure $TiO_2$ nanoparticles: anatase, brookite and rutile," *Nanotechnology*, vol. 19, no. 14, Article ID 145605, 2008.

[46] N. Serpone, D. Lawless, and R. Khairutdinov, "Size effects on the photophysical properties of colloidal anatase $TiO_2$ particles: size quantization or direct transitions in this indirect semiconductor?" *Journal of Physical Chemistry*, vol. 99, no. 45, pp. 16646–16654, 1995.

[47] E. Sanchez and T. Lopez, "Effect of the preparation method on the band gap of titania and platinum-titania sol-gel materials," *Materials Letters*, vol. 25, no. 5-6, pp. 271–275, 1995.

[48] D. S. Bhatkhande, V. G. Pangarkar, and A. Beenackers, "Photocatalytic degradation for environmental applications—a review," *Journal of Chemical Technology and Biotechnology*, vol. 77, no. 1, pp. 102–116, 2002.

[49] W. R. Zhao, H. X. Shi, and D. H. Wang, "Ozonation of Cationic Red X-GRL in aqueous solution: degradation and mechanism," *Chemosphere*, vol. 57, no. 9, pp. 1189–1199, 2004.

[50] A. Demirev and V. Nenov, "Ozonation of two acidic azo dyes with different substituents," *Ozone: Science & Engineering*, vol. 27, no. 6, pp. 475–485, 2005.

[51] M. Stylidi, D. I. Kondarides, and X. E. Verykios, "Visible light-induced photocatalytic degradation of Acid Orange 7 in aqueous $TiO_2$ suspensions," *Applied Catalysis B*, vol. 47, no. 3, pp. 189–201, 2004.

[52] Y. Mu, H. Q. Yu, J. C. Zheng, and S. J. Zhang, "$TiO_2$-mediated photocatalytic degradation of Orange II with the presence of $Mn^{2+}$ in solution," *Journal of Photochemistry and Photobiology A*, vol. 163, no. 3, pp. 311–316, 2004.

[53] I. K. Konstantinou and T. A. Albanis, "$TiO_2$-assisted photocatalytic degradation of azo dyes in aqueous solution: kinetic and mechanistic investigations: a review," *Applied Catalysis B*, vol. 49, no. 1, pp. 1–14, 2004.

[54] Q. L. Yu, M. M. Ballari, and H. J. H. Brouwers, "Indoor air purification using heterogeneous photocatalytic oxidation. Part II: kinetic study," *Applied Catalysis B*, vol. 99, no. 1-2, pp. 58–65, 2010.

[55] V. Houăková, V. Štengl, S. Bakardjieva, N. Murafa, and V. Tyrpekl, "Photocatalytic properties of Ru-doped titania prepared by homogeneous hydrolysis," *Central European Journal of Chemistry*, vol. 7, no. 2, pp. 259–266, 2009.

[56] J. Wang, X. Liu, R. Li, P. Qiao, L. Xiao, and J. Fan, "$TiO_2$ nanoparticles with increased surface hydroxyl groups and their improved photocatalytic activity," *Catalysis Communications*, vol. 19, pp. 96–99, 2012.

[57] V. B. R. Boppana and R. F. Lobo, "Photocatalytic degradation of organic molecules on mesoporous visible-light-active

Sn(II)-doped titania," *Journal of Catalysis*, vol. 281, no. 1, pp. 156–168, 2011.

[58] Y. Zhao, J. Liu, L. Y. Shi et al., "Surfactant-free synthesis uniform $Ti_{1-x}Sn_xO_2$ nanocrystal colloids and their photocatalytic performance," *Applied Catalysis B*, vol. 100, no. 1-2, pp. 68–76, 2010.